Nanoscale

Accepted Manuscript

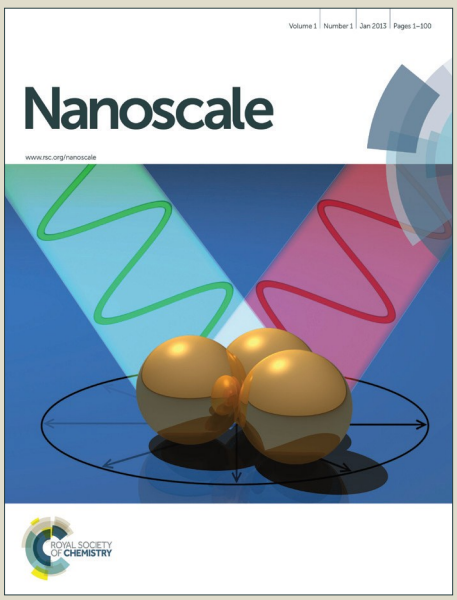

ROYAL SOCIETY OF CHEMISTRY

www.rsc.org/nanoscale

Growth, Patterning and Alignment of Organolead Iodide Perovskite Nanowires for Optoelectronic Devices

Hui Deng[1], Dongdong Dong[1], Keke Qiao[1], Lingling Bu[1], Bing Li[1], Dun Yang[1], Hong-En Wang[2], Yibing Cheng[1, 3], Zhixin, Zhao[1], Jiang Tang[1], Haisheng Song[1*]*

[1]Wuhan National Laboratory for Optoelectronics (WNLO) and School of Optical and Electronic Information, Huazhong University of Sciences and Technology, 1037 Luoyu Road, 430074, Wuhan, Hubei, P. R. China

[2]State Key Laboratory of Advanced Technology for Materials Synthesis and Processing, Wuhan University of Technology, Luoshi Road, 430070, Wuhan, Hubei, China

[3]Department of Materials Engineering, Monash University, Melbourne, Victoria, 3800, Australia

[*]Email of corresponding authors: zhixin-zhao@163.com and songhs-wnlo@mail.hust.edu.cn

Abstract

Organolead halide perovskites are becoming intriguing materials applied in optoelectronics. In present work, Organolead iodide perovskite (OIP) nanowires (NWs) have been fabricated by one step self-assembly method. The controllable NW distributions were implemented by a series of facile techniques: monolayer and small diameter NWs were carried out by precursor concentration tuning; NW patterning was achieved via selected area treatment assisted by mask; NW alignment was implemented by modified evaporation-induced self-assembly (EISA). The synthesized multifunctional NWs were further applied in photodetectors (PDs) and solar cells as application demos. The PD performances have reached the order of A/W for responsivity, 10^{12} jones for detectivity and less than one millisecond for response speed, superior to OIP film and other typical inorganic NWs based PD performances. Energy conversion efficiency of ~2.5% has been obtained for NW film based solar cells. The facile fabrication process, controllable distribution and optoelectronic applications make the OIP NWs as promising building blocks for future optoelectronics especially for low dimensional devices.

Key words： Perovskite; nanowires; evaporation-induced self-assembly; controllable distribution; optoelectronics

Introduction

Organolead halide perovskites based optoelectronic devices are attracting intense research interest due to their low cost, mild fabrication process, high energy conversion efficiency and tunable optoelectronic properties.[1-4] The reported organolead halide perovskite thin film for optoelectronic devices is mostly cast from nanoparticle or micron size grain by various novel techniques.[4] To date, the controlling crystallization utilizes a two-step sequential deposition or one step crystallization with fast deposition induced by anti-solvent additive in solution method.[5-7] The products of one step solution method contain large amount of dendrite-like whiskers in spin coating. The dendrite crystal growth implies that organolead iodide perovskite (OIP) contains preferential growth. Inspired from that, the synthesis of OIP NWs were investigated and implemented in the present work. For OIP material properties, first-principle calculations demonstrate the unusual defect physics in which the dominant defects are shallow levels.[8] The benign defect physics was further confirmed by solar cell performances where there was no apparent offset between nanoparticle and large micron size based devices.[5, 7] The benign defects of OIP materials and expected superior charge transport properties of single crystal NWs promise the OIP NWs wide applications in not only thin film solar cells but also low dimensional optoelectronic devices. Compared with thin film solar cell investigation, other morphologies and applications are limited for OIP materials.

Single crystalline semiconductor NWs have been extensively studied in last few decades due to their unique electronic and optical properties and potential applications in special electronic and photonic devices.[9] The unique properties of NWs arise attributed to their anisotropic geometry, large surface to volume ratio, and carrier and photon confinement in two dimensions (1D system). [10-12] In most case, self-assembled NWs in solution method tend to distribute in a macroscopically random style on substrates. The disordered NWs may lead to poor device performance and low NW utilization due to the mismatch distribution between the random NWs and the traditional ordered electrodes.[13] Therefore, a uniform distribution, patterning and

alignment for OIP NWs are highly desired for optoelectronics.

Several strategies for NW alignment have been reported, such as the Langmuir–Blodgett technique, [14, 15] electric or magnetic field assisted alignment, [16, 17] dip coating, [18, 19] electrostatic alignment[20] and so on. However, those techniques usually become invalid in large-area ordered patterns. In contrast, evaporation-induced self-assembly method (EISA) has been widely utilized for large scale aligned NW patterns. In present OIP NW alignment, tilted substrate growth combining with EISA method (modified EISA method) were applied to guide the alignment of NW growth. For NW patterning, NW distribution area highly depends on the solution distribution. Once the substrate surface is selectively treated into hydrophilic, the solution can uniformly spread out only on treated area. In present work, UV-ozone treatment combined with shadow mask was utilized for the NW patterning.

Herein, OIP NWs were fabricated by one step self-assembly solution method. Uniform NW distribution, patterning deposition and NW alignment were carried out on common substrates (glass, SiO_2/Si, FTO). Two kinds of optoelectronic devices were fabricated based on OIP NWs. One was photodetector (PD) utilizing monolayer NW as low dimensional device demos, and the other was NW film solar cells as thin film device demonstration. Performances of PDs were superior to the reported thin film based PDs[21] and the photovoltaic devices could work with ~2.5% conversion efficiency. The investigation of present OIP NWs based work is expected to open the window for the OIP NW applications in optoelectronic fields.

Methods

Perovskite NW growth. Unless otherwise indicated, all starting materials were obtained from commercial suppliers and used without further purification. CH_3NH_3I was synthesized according to a previous study[22]. The precursor solution was prepared by mixing of equimolar of PbI_2 and CH_3NH_3I DMF solution. The starting concentration was 45 wt% and the other varied concentrations were obtained by diluting 45 wt% solution. Substrates were ultrasonically degreased by sequential washing solution of acetone, ethanol, DI water and boiled H_2SO_4:H_2O_2 (5:2) solution.

For NW growth experiments, four pieces of clean glass substrate were preheated by four hot plates and the setting temperature was 120 °C, 90 °C, 60 °C and RT, respectively. Ten micron-liter of 45 wt% perovskite solution were dropped to above four preheated substrates. Solution coated substrates were kept on hot plate for 3 hour and the substrates gradually became light black. Finally, the light black products were annealed at 80 °C for 10 min to obtain the NWs. Besides this part, the following NWs were all grown at RT and annealed at 80 °C for 10 min.

Controllable distribution of OIP NWs: A UV-ozone treatment was utilized to make the substrate surface hydrophilic for uniform distribution and the power was set at 500 W and duration time was 30 min. The contact angle was tested by a contact angle meter (USA Kino Industry SL200B). The fixed volume ~1 μL solution was dropped to the treated substrate for NW growth. Four kind concentrations of 45 wt%, 10 wt%, 1 wt%, 0.1 wt% were dropped to SiO_2/Si substrates to investigate the concentration effects to NW growth. Three-step method as shown in Fig. 4b was utilized for NW patterning growth. SiO_2/Si substrates coated by 1 μL 2 wt% solution were tilted to a small angle (~ 10 °) for aligned NW experiments. The prepared OIP NWs were characterized by scanning electron microscopy (SEM, Nova NanoSEM 450), HRTEM (Tecnai G^2 20 U-Twin), XRD (XRD-7000S/L) and UV-Vis absorption spectra (Cary, Lambda 950).

Photodetector fabrication and measurements. The aligned perovskite NWs uniformly distributed on SiO_2/Si or glass substrates were patterned with interdigitated Au electrodes by thermal evaporation assisted with a shadow mask. The active channels were 350 μm in width and 1.5 cm in length. Photodetector performances were measured using a probe station connected to an Agilent B1500A semiconductor characterization system. The device was further covered with an aluminum cap to provide optical and electromagnetic shielding. Illumination was generated from monochromatic light-emitting diodes controlled by a functional generator (Agilent 33210A). Light intensity was calibrated using a Silicon photodetector (Newport 818-UV).

Soalr cell fabrication and measurements. The NW thin film solar cells were fabricated same as the typical device fabrications except absorbed materials[23]. The device configuration was FTO/dense TiO_2 layer/mesoporous TiO_2 layer/OIP NW film/hole transport layer (HTM)/Au. The OIP NW layer was deposited the same as aforementioned NW growth part and the only difference was spraying solution onto the substrates for fast deposition instead of dropping. A sun simulator (Oriel) coupled with a filtered 1,000W xenon lamp was used to provide simulated solar irradiation (AM1.5, 100mW/cm^2). Current-voltage characteristics were measured using a Keithley 2400 meter.

Results and discussions

Preferential growth of NWs. The precursor concentrations firstly referred to thin film solar cell fabrication technique of one step method.[24] A droplet of 45 wt% precursor solution (constant volume, 10 μL) of equimolar CH_3NH_3I and PbI_2 in dimethyl formamide (DMF) was dropped onto FTO substrates by pipette. Figure 1a-d showed the product morphologies affected by the varied substrate temperature (120 °C, 90 °C, 60 °C and RT (room temperature)). The corresponding morphologies were nanoparticles, mixtures of nanowhiskers and nanoparticles, nanowires, respectively. The high-resolution transmission electron microscopy (HRTEM) image of single NW was shown in Fig. 1e and the space of the lattice fringe was ~0.31 nm. As shown in HRTEM image, the whole crystals grew along the same axis direction which was further confirmed by fast Fourier transform (FFT) images of two different selected areas (denoted as f and g). Figure 1f and 1g showed almost the same perovskite diffraction spots. Consequently, the NW was single crystal and the growth direction was [100]. The obtained NWs were further characterized by x-ray diffraction (XRD) and the XRD spectra (Fig. 1h) agreed well with the tetragonal perovskite spectra[25] no matter the NWs were deposited on glass (1#), FTO substrates (2#) or SiO_2/Si substrates (3#).

The growth procedure of present NW growth method could be described as evaporation-induced self-assembly. When the precursor solution was cast on

substrates, the evaporation of solvent resulted in the supersaturated crystals growth with the *c-axis* paralleling to the surface at RT.[26] The low symmetry (tetragonal *I4/mcm*) of OIP and strong intermolecular interactions may allow for a preferred growth into NW morphology[27, 28]. For high substrate temperature of 120 °C (Fig.1a), it tended to grow homogeneously into nanoparticles [29] and suppress the preferential growth. While growing at RT (Fig.1d), the natural evaporation preferentially grew into NWs due to the low symmetry structure similar to reported spin coating process[26, 30].

Uniform NW distribution. In addition to the right crystal phase of perovskite NWs, the NW distribution on substrate should match the traditional techniques of micro- and nano-fabrications. The uniform distribution was implemented by UV-ozone treatment due to the improvement of surface DMF infiltration. The contact angles of SiO_2/Si substrates before (Fig. 2a) and after (Fig. 2b) the UV-ozone treatments were 71° and 3°, respectively. The surface treatment significantly decreased the contact angle and improved the substrate infiltration. Once 1 μL solution was dropped onto the treated substrate, it quickly spread out to whole substrate (~1.5 cm^2). The uniform distribution of solution and low evaporation speed (natural evaporation at RT) insured the uniform distribution of following NW growth in whole substrate. The treatment was also applied to other common substrates, and it was found that such treatment was not sensitive to substrate material. Figure 2c and 2d showed the NW distribution on non-treated and UV-ozone treated SiO_2/Si substrates, respectively. Nanowires on treated substrate uniformly distributed on whole substrate without any NW aggregation (Fig. 2d). In contrast, NWs on non-treated substrates aggregated into bundle-like morphologies and some places were blank (Fig. 2c).

The effect of precursor concentration. As aforementioned part utilizing 45 wt% starting precursor concentration, multilayer NW products were obtained. The varied number of NW layers greatly affects their applications in low dimensional devices.[9] Precursor concentrations were investigated to tune the number of layers and NW

diameters. Figure 3a-d showed the NW products grown from precursor concentrations of 45 wt%, 10 wt%, 1 wt% and 0.1 wt%, respectively. The following statistic number of NW layer and diameter were roughly estimated. The decreasing concentrations resulted in the decreased number of layers and diameters. The number of layers and diameters for Figure 3a and 3b (45 wt% and 10 wt% concentrations) were 4-8 layers and 0.5-1 μm, 2-5 layers and 0.3-0.8 μm, respectively. Monolayer NWs were obtained when the precursor concentrations were not higher than 1 wt% (Fig. 3c and 3d). The corresponding NWs also showed smaller diameter and less than 100 nm could be obtained when the concentrations didn't exceed 0.1 wt%. The evolved trends of layers and diameters mainly attributed to natural evaporation induced self-assembly growth. Nanowire growth mainly contained two processes, nucleation and crystal growth. Following the solvent evaporation, solute concentration gradually increased. When the concentration arrived to supersaturation, nucleation occurred and crystal growth would also happen in an inseparable process. Because of the natural evaporation of present growth, the nucleation and growth were coupled to each other as the solvent evaporation[29, 31]. For high concentration precursor, the nucleation and growth cycled for many times led to multilayer NWs and wider diameter distribution. While for low concentration precursors, the supersaturated concentration was difficult to meet and the nucleus only occurred in a short time. Thus, the corresponding products contained monolayer NWs with smaller diameters.

Nanowire patterning. Nanowires only growing on selected area not only increase the NW utilization efficiency but also avoid contamination on non-desired area. The present NW patterning was implemented by UV-ozone treatment assisted by shadow mask. Figure 4a described the schematic image of selected area NW growth. Substrates covered by mask were firstly treated by UV-ozone to ensure the selected area hydrophilic (Step 1). After dropping the solution on non-masked substrate, the solution only dispersed on treated area (Step 2). Finally, NWs only grew on treated area and the selected area growth was achieved (Step 3). Figure 4b and 4c showed the selected area growth results and NWs only grew on rectangular treated area with

sharp edge. Those demonstrated that the present treatment assisted by mask method could efficiently work for NW patterning. The patterning work avoiding the utilization of traditional photolithography and photoresist are expected to greatly broaden the OIP NW application fields and simplify the device fabrication process.

Nanowire alignment. The growth products of OIP NWs on UV-ozone treated surface distributed uniformly and randomly as shown in Fig. 5a. The disordered distribution mismatched the traditional ordered electrodes for device applications. Evaporation induced self-assembly method has been successfully utilized in synthesis of ordered organic NWs[32-34]. The EISA method was firstly applied for present NW aligned growth, and the aligned NW area was small especially in center area where NWs randomly distributed (not shown here). In order to obtain large area aligned NW distribution such as whole substrate, the substrates were tilted for a small angle less than 15° to guide the NW alignment. The growth mechanism was schematically described in Fig. 5b. Utilizing the present modified EISA method (EISA combining with tilted substrate growth), NWs in whole substrate aligned very well quasi-vertically to the substrate edge. Figure 5c and 5d described the NW distribution in two different positions, one was the starting growth area, substrate edge (Fig. 5c) and the other was the area far from the edge (Fig. 5d). Both of them aligned to the same direction along the evaporation direction (arrowed in Fig. 5b) which demonstrated the well aligned growth in whole substrate. For the growth mechanism described in Fig. 5b, nanowires started growth from the substrate edge due to the heterogeneous nucleation growth[30]. As the evaporation continuing, contact line (liquid/substrate interface) driven by evaporation and gravity moved along the evaporation direction. In other words, the evaporation direction can help to guide the NW growth in whole substrate. As a result, the modified EISA method could be utilized for large scale ordered NW growth. This alignment effect can also be explained by energetically favorable and surface energy minimization growth[35].

Photodetectors (PDs) of monolayer NWs. Monolayer aligned NWs were firstly applied in PDs as low dimensional optoelectronic device demos. Absorption of NW

film was measured by UV-vis spectra as shown in Fig. 6a. Such NW film (~ 300 nm thickness) can absorb more than 90% of the light from UV to whole visible light consistent to its bandgap and high molar extinction coefficient[4]. The broadband absorption and high absorption coefficient promise the present NWs as superior material for high performance PDs. The inset of Fig. 6b showed the optical micrograph of the fabricated conductive PD. The average diameter and length of the NWs were 500 nm and 800 μm, respectively. The lighted current (I_{light}) *versus* applied bias curves were shown in Fig. 6b under light irradiance of different wavelength. At a constant light intensity (~ 80 μW/cm^2), PDs excited by 650 nm light obtained larger I_{light}. Concerning that, the left work utilizes 650 nm light for illumination if not specially specified. Figure 6c showed the I-t curve under the repetitive switching of 650 nm light at a bias of 2 V. The I_{light} and I_d (dark current) were stable as the reversible and rapid switch between the illuminated state and dark state. The obtained I_{light} and I_d were 115 nA and 5 nA, respectively and a I_{light} / I_d ratio can arrived at 23. From high resolution scan of one cycle of I-t curves as shown in Fig. 6d, the extracted rise and decay time were 0.2 ms and 0.3 ms, respectively which were superior to reported thin film based PD's speed (~ 100 ms)[21].

For a conductive photodetector, detectivity (D^*) and responsivity (R) are the figures of merit to compare the performances of different geometry devices. Detectivity is defined by responsivity, device area (A), electrical bandwidth (B) and noise current (I_n) through the equation: $D^* = \frac{R\sqrt{AB}}{I_n}$. Responsivity is defined by photocurrent ($I_p = I_{light} - I_d$) divided by the incident power (P) to the active area. The shot noise, associated with current fluctuation flowing across a PD, often dominates the total noise of the detector[36]. So I_n could be approximately correlated with I_d described by $I_n = \sqrt{2qI_dB}$ where q is elementary charge. Therefore, D^*can be simplified as $D^* = \frac{I_p\sqrt{A}}{P\sqrt{2qI_d}}$. In Fig. 7a, I_p increased as the applied voltage and irradiation increased which roughly reflected the depending relationship among I_p, applied bias

and *P*. Figure 7b and 7c further showed the detailed responsivity evolution as changed bias and irradiation, respectively. The estimated *R* can arrive to 1.3 A/W as the increase of applied bias under a fixed illumination of 80 μW/cm^2. In contrast, *R* increased to 0.85 A/W at a fixed bias of 1V when the illumination decreased to 4 μW/cm^2. Considering the evolution of Fig. 7b and 7c, it can be concluded that higher bias and lower irradiance can obtain higher *R* than present 1.3 A/W. Similar trend was also observed for D^*-*P* curve (Fig. 7d) and the estimated detectivity can arrive at 2.5×10^{12} Jones at a bias of 1 V. The present PDs have also been measured by higher bias voltage to confirm the PD stability. From Figure S2 in Supporting Information, the PDs can stand under 50 V testing. Compared with recent OIP film[21] and low dimensional inorganic NWs based PDs[37, 38], the performances of present PDs demonstrated superior response time, responsivity and detectivity which promised it as high potential in light sensor applications. The single crystal structure, high light absorption coefficient and good ohmic contact ensured the superior performances of the present PDs.

Solar cells of NW film. The other demo based on OIP NW thin film solar cells has also been fabricated. There are double layers of perovskite material contained in solar cells. One layer is perovskite nanoparticles infiltrated into the mesoporous TiO_2 layer and the other is the left NWs capping the whole TiO_2 surface (Supporting Information Figure S3). As shown in Fig. 8, the measured key parameters of open circuit voltage (V_{oc}), short-circuit current density (J_{sc}), filled factor (*FF*) and power conversion efficiency (PCE) were 0.75 V, 5.4 mA/cm^2, 61% and 2.5%, respectively. Compared with the reported high efficiency (~19.3%) of OIP thin film solar cells[4-6], the obtained J_{sc} were much lower because of the thicker film required to avoid shorting of the inter-NW void. On the other hand, the non-full fill of NWs may find the applications in semi-transparent solar cells. The prototype devices manifested the implementation of OIP NW solar cells and need further optimization.

It was noted that another paper also reported the OIP NW growth[39] during the preparing manuscript process of present work. The size distribution of NWs

synthesized by slip-coating method and random NW based PDs have been investigated. The superior charge carrier extraction in NW based devices has also been expected.

Conclusions

A new morphology of OIP materials, OIP NW, has been successfully implemented. The self-assembly growth NWs mainly attributed to the low symmetry of OIP and the strong intermolecular interactions. As one kind of low dimensional materials for optoelectronic devices, controllable distribution of NWs was crucial for its applications. The NW patterning and alignment were implemented by selected area treatment and modified EISA, respectively. The synthesized NWs were successfully applied in low dimensional PDs and thin film solar cells as demos. Monolayer NWs based PDs obtained a response time of ~ 0.3 ms, a responsivity of 1.3 A/W and a detectivity of 2.5×10^{12} Jones, which are superior to recent reported PD performances based on OIP thin film and inorganic NWs. Thin film solar cells based on OIP NW also worked and obtained an energy conversion efficiency of 2.5%. The one dimensional single crystal, mild growth conditions, controllable distribution and superior light absorption and conversion properties promise the present NWs wide applications in optoelectronics.

Supporting Information

The leakage current level of PDs, I-t curves of PDs at high bias voltage and the surface morphologies of NW absorption layer have been listed in supporting information materials.

Acknowledgement

This work was financially supported by the National Natural Science Foundation of China (61306137), the Fundamental Research Funds for the Central Universities (HUST： 2014QN014) and the financial support by 973 Program of China (2011CBA00703). The authors thank Testing Center of HUST and the Center for

Nanoscale Characterization and Devices, Wuhan National Laboratory for Optoelectronics (WNLO) for facility access.

Reference

1. G. Hodes, *Science*, 2013, **342**, 317-318.
2. N.-G. Park, *J. Phys. Chem. Lett.*, 2013, **4**, 2423-2429.
3. H. J. Snaith, *J. Phys. Chem. Lett.*, 2013, **4**, 3623-3630.
4. P. Gao, M. Gratzel and M. K. Nazeeruddin, *Energ. Env. Sci.*, 2014, **7**, 2448-2463.
5. J. Burschka, N. Pellet, S. J. Moon, R. Humphry-Baker, P. Gao, M. K. Nazeeruddin and M. Gratzel, *Nature*, 2013, **499**, 316-319.
6. Q. Chen, H. Zhou, Z. Hong, S. Luo, H. S. Duan, H. H. Wang, Y. Liu, G. Li and Y. Yang, *J. Am. Chem. Soc.*, 2014, **136**, 622-625.
7. M. Xiao, F. Huang, W. Huang, Y. Dkhissi, Y. Zhu, J. Etheridge, A. Gray-Weale, U. Bach, Y. B. Cheng and L. Spiccia, *Angew. Chem. Int. Ed. Engl.*, 2014, **53**, 10056-10061.
8. W.-J. Yin, T. Shi and Y. Yan, *Appl. Phys. Lett.*, 2014, **104**, 063903.
9. R. Agarwal and C. M. Lieber, *Appl. Phys. A-mater.*, 2006, **85**, 209-215.
10. X. Duan, Y. Huang, R. Agarwal and C. M. Lieber, *Nature*, 2003, **421**, 241-245.
11. C. J. Barrelet, A. B. Greytak and C. M. Lieber, *Nano Lett.*, 2004, **4**, 1981-1985.
12. O. Hayden, R. Agarwal and C. M. Lieber, *Nat. Mater.*, 2006, **5**, 352-356.
13. S. C. Mannsfeld, A. Sharei, S. Liu, M. E. Roberts, I. McCulloch, M. Heeney and Z. Bao, *Adv. Mater.*, 2008, **20**, 4044-4048.
14. A. Tao, F. Kim, C. Hess, J. Goldberger, R. He, Y. Sun, Y. Xia and P. Yang, *Nano Lett.*, 2003, **3**, 1229-1233.
15. P. Yang, *Nature*, 2003, **425**, 243-244.
16. G. Piao, F. Kimura and T. Kimura, *Langmuir*, 2006, **22**, 4853-4855.
17. M. Li, R. B. Bhiladvala, T. J. Morrow, J. A. Sioss, K.-K. Lew, J. M. Redwing, C. D. Keating and T. S. Mayer, *Nat. Nanotechnol.*, 2008, **3**, 88-92.
18. N. Liu, Y. Zhou, L. Wang, J. Peng, J. Wang, J. Pei and Y. Cao, *Langmuir*, 2008, **25**, 665-671.
19. C. Zhang, X. Zhang, X. Zhang, X. Fan, J. Jie, J. C. Chang, C.-S. Lee, W. Zhang and S.-T. Lee, *Adv. Mater.*, 2008, **20**, 1716-1720.

20. A. M. Kalsin, M. Fialkowski, M. Paszewski, S. K. Smoukov, K. J. M. Bishop and B. A. Grzybowski, *Science*, 2006, **312**, 420-424.

21. X. Hu, X. Zhang, L. Liang, J. Bao, S. Li, W. Yang and Y. Xie, *Adv. Funct. Mater.*, DOI:10.1002/adfm.201402020.

22. J. H. Im, C. R. Lee, J. W. Lee, S. W. Park and N. G. Park, *Nanoscale*, 2011, **3**, 4088-4093.

23. H. S. Kim, C. R. Lee, J. H. Im, K. B. Lee, T. Moehl, A. Marchioro, S. J. Moon, R. Humphry-Baker, J. H. Yum, J. E. Moser, M. Gratzel and N. G. Park, *Sci. Rep.*, 2012, **2**, 591-597.

24. L. Etgar, P. Gao, Z. Xue, Q. Peng, A. K. Chandiran, B. Liu, M. K. Nazeeruddin and M. Gratzel, *J. Am. Chem. Soc.*, 2012, **134**, 17396-17399.

25. J. H. Heo, S. H. Im, J. H. Noh, T. N. Mandal, C.-S. Lim, J. A. Chang, Y. H. Lee, H.-j. Kim, A. Sarkar, K. NazeeruddinMd, M. Gratzel and S. I. Seok, *Nat. Photonics*, 2013, **7**, 486-491.

26. Y. Tidhar, E. Edri, H. Weissman, D. Zohar, G. Hodes, D. Cahen, B. Rybtchinski and S. Kirmayer, *J. Am. Chem. Soc.*, 2014, **136**, 13249-13256.

27. T. Baikie, Y. Fang, J. M. Kadro, M. Schreyer, F. Wei, S. G. Mhaisalkar, M. Graetzel and T. J. White, *J. Mater. Chem. A*, 2013, **1**, 5628-5641.

28. C. C. Stoumpos, C. D. Malliakas and M. G. Kanatzidis, *Inorg. Chem.*, 2013, **52**, 9019-9038.

29. J. A. Dirksen and T. A. Ring, *Chem. Eng. Sci.*, 1991, **46**, 2389-2427.

30. A. Cacciuto, S. Auer and D. Frenkel, *Nature*, 2004, **428**, 404-406.

31. F. Huang, Y. Dkhissi, W. Huang, M. Xiao, I. Benesperi, S. Rubanov, Y. Zhu, X. Lin, L. Jiang, Y. Zhou, A. Gray-Weale, J. Etheridge, C. R. McNeill, R. A. Caruso, U. Bach, L. Spiccia and Y.-B. Cheng, *Nano energy*, 2014, **10**, 10-18.

32. R. D. Deegan, O. Bakajin, T. F. Dupont, G. Huber, S. R. Nagel and T. A. Witten, *Phys. Rev. E*, 2000, **62**, 756.

33. R. D. Deegan, O. Bakajin, T. F. Dupont, G. Huber, S. R. Nagel and T. A. Witten, *Nature*, 1997, **389**, 827-829.

34. C. J. Brinker, Y. Lu, A. Sellinger and H. Fan, *Adv. Mater.*, 1999, **11**, 579-585.

35. G. E. Eperon, V. M. Burlakov, P. Docampo, A. Goriely and H. J. Snaith, *Adv. Funct. Mater.*, 2014, **24**, 151-157.

36. E. Heves, C. Ozturk, V. Ozguz and Y. Gurbuz, *Ieee Electron Device Letters*, 2013, **34**, 662-664.

37. F.-X. Wang, J. Lin, W.-B. Gu, Y.-Q. Liu, H.-D. Wu and G.-B. Pan, *Chem. Commun.*, 2013, **49**, 2433-2435.

38. G. Chen, Z. Liu, B. Liang, G. Yu, Z. Xie, H. T. Huang, B. Liu, X. F. Wang, D. Chen, M. Q. Zhu and G. Z. Shen, *Adv. Funct. Mater.*, 2013, **23**, 2681-2690.

39. E. Horváth, M. Spina, Z. Szekrényes, K. Kamarás, R. Gaal, D. Gachet and L. Forró, *Nano Lett.*, 2014, **14**, 6761–6766.

Figure captions:

Fig. 1 NW growth. (a-d) SEM morphologies prepared at different substrate temperatures. (a) 120 °C, (b) 90 °C, (c) 60 °C and (d) RT. (e-g) HRTEM image of single NW (e) and its selected area FFT patterns (f and g). The FFT patterns were extracted from different circled areas denoted as f and g in (e). (h) The XRD spectra of the obtained NWs on different substrates. The spectra denoted as 1#, 2# and 3# were measured from the NWs grown on glass, FTO and SiO_2/Si substrates. Star marks pointed out the standard perovskite XRD peaks. Solid circles indicated the XRD peaks from FTO.

Fig. 2 Surface treatment effects. (a, b) Optical images of contact angle measurements taken from the non-treated substrates and UV-ozone treated substrates. Their contact angles were 71° and 3°, respectively. (c, d) Optical images of growth products from non-treated substrates and treated substrates, respectively.

Fig. 3 Growth products synthesized from different concentrations. (a) 45 wt%, (b) 10 wt%, (c) 1 wt%, (d) 0.1 wt%.

Fig. 4 NW patterning growth. (a) Schematic description for the selected area growth. (b, c) SEM images from three neighbor selected area (b) and one integrated area (c).

Fig. 5 NW alignment growth. (a) SEM image of randomly distributed NWs. (b) Schematic description for the aligned NW growth. Evaporation direction was pointed out by arrows. (c, d) Optical images of NWs grown by modified EISA method. The patterns were captured from substrate edge (c) and remote area from edge (d).

Fig. 6 (a) UV-Vis spectra of OIP NW film. (b) photocurrent response under different wavelength light illumination from UV to infrared. Inset was the optical image of a typical PD with a scale bar of 200 μm. (c) I-t curve illuminated by 650 nm light at a bias of 2 V. (d)High resolution scan to one cycle of I-t curves. The time interval was 0.1 ms.

Fig. 7 (a) I-V curves under different illumination power densities at a bias of 1 V. (b) PD responsivity depending on the applied bias under 650 nm light illumination at a power density of 80 $\mu W/cm^2$. (c) Depending relationship between responsivity and

irradiance at a fixed bias of 1 V. (d) The normalized detectivity evolved as the irradiance and the applied bias was 1 V.

Fig. 8 Photocurrent density of solar cells as a function of the forward bias voltage. Inset was the detailed performance parameters.

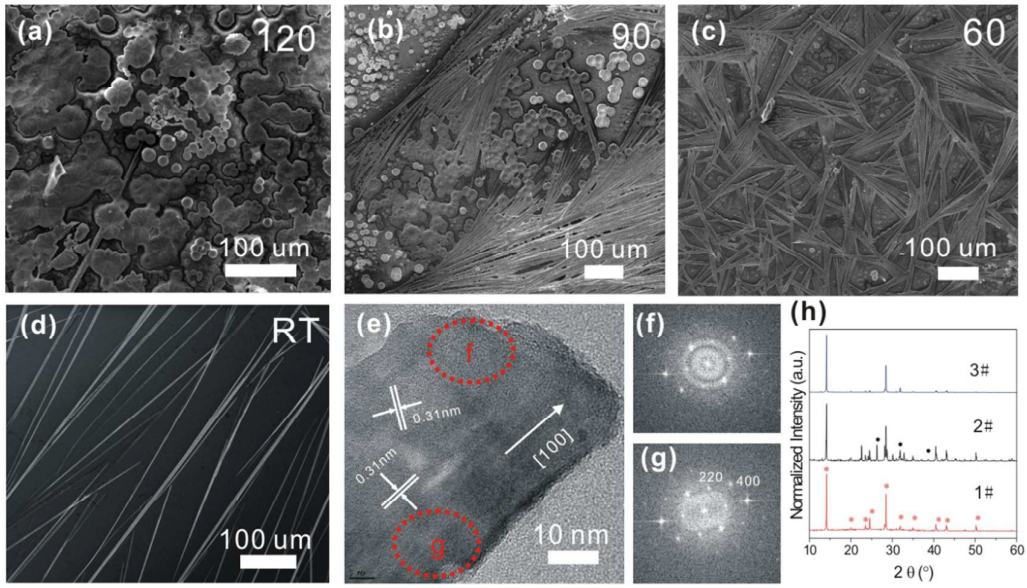

Fig. 1

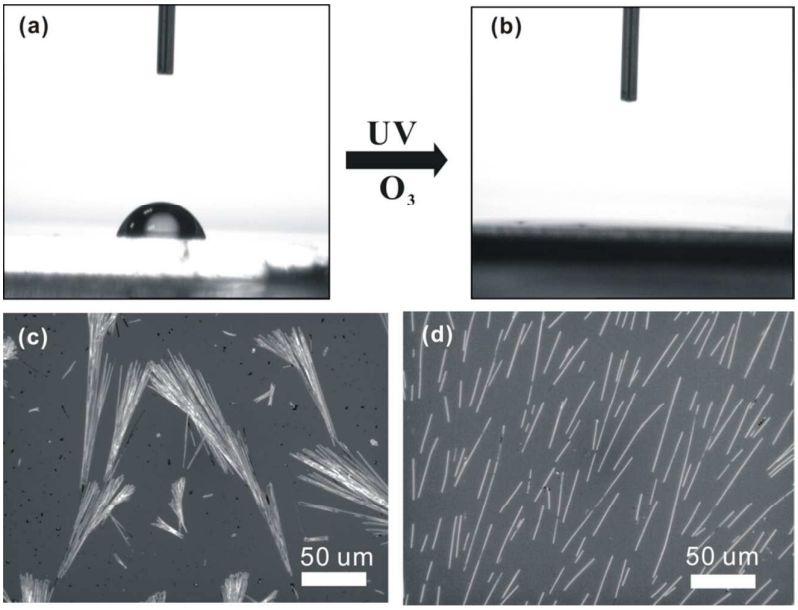

Fig. 2

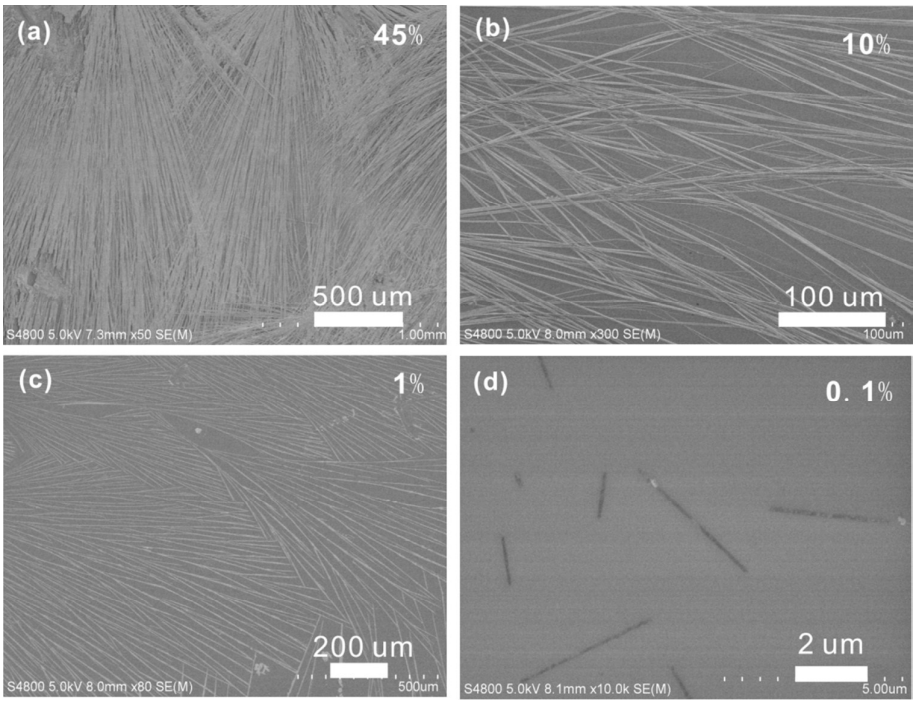

Fig. 3

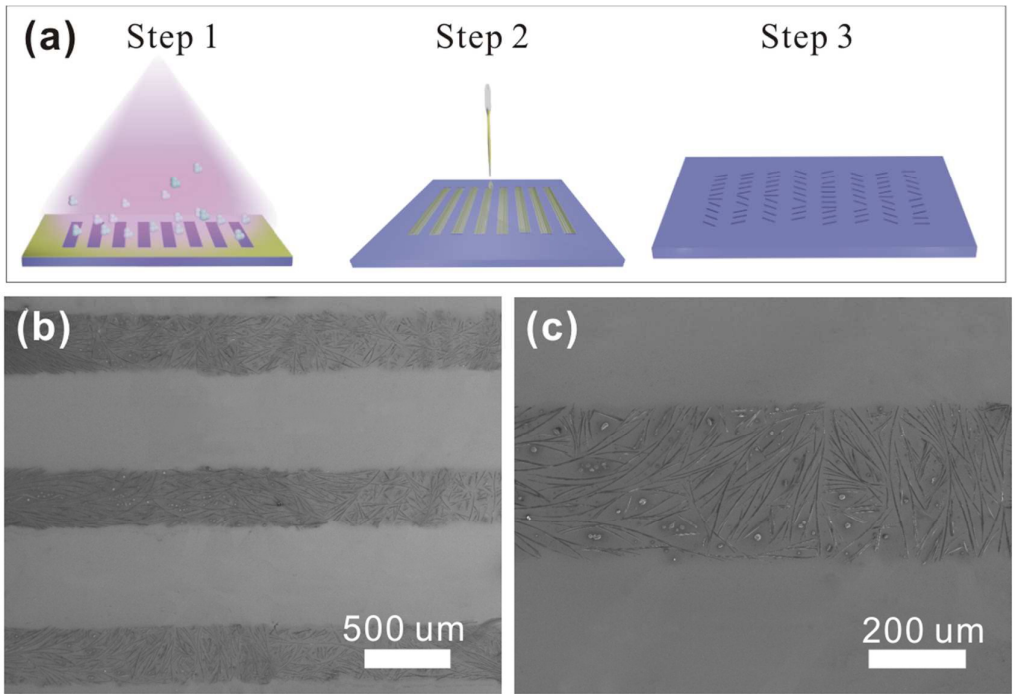

Fig. 4

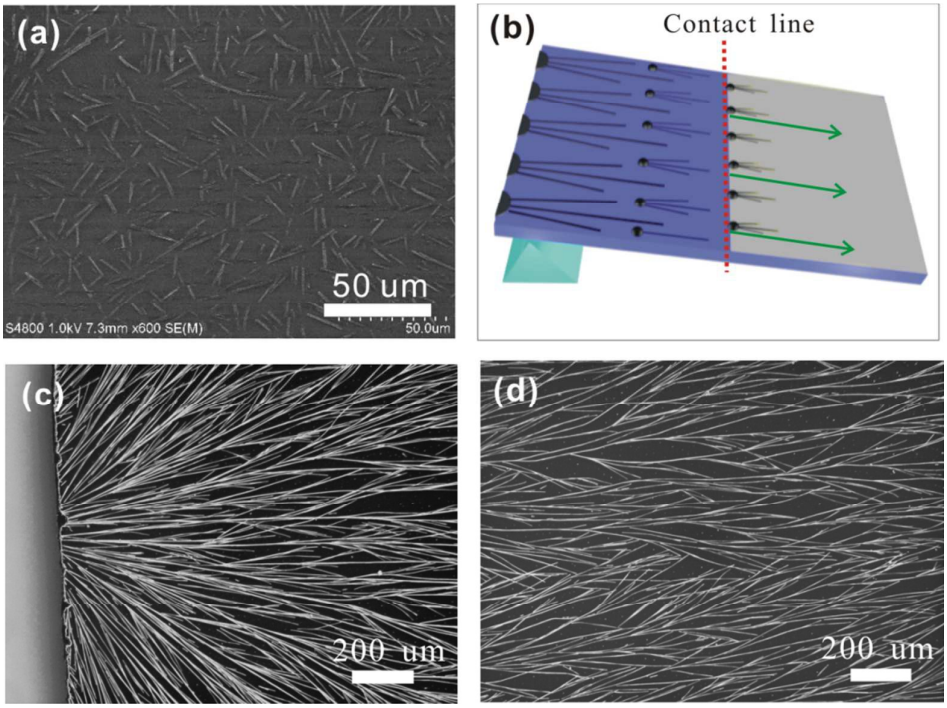

Fig. 5

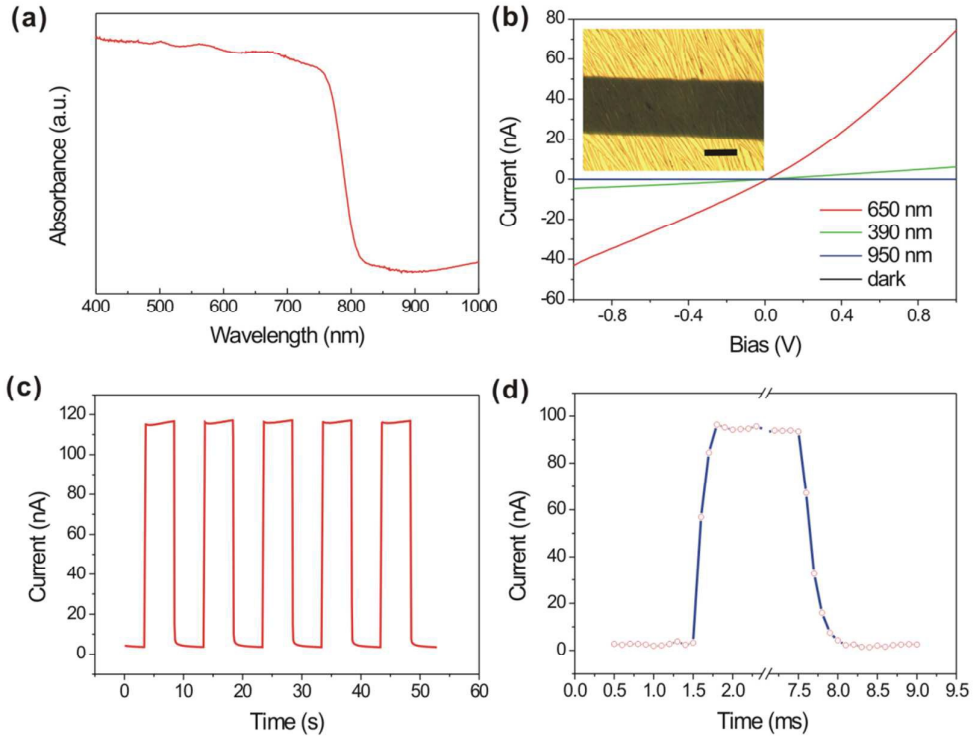

Fig. 6

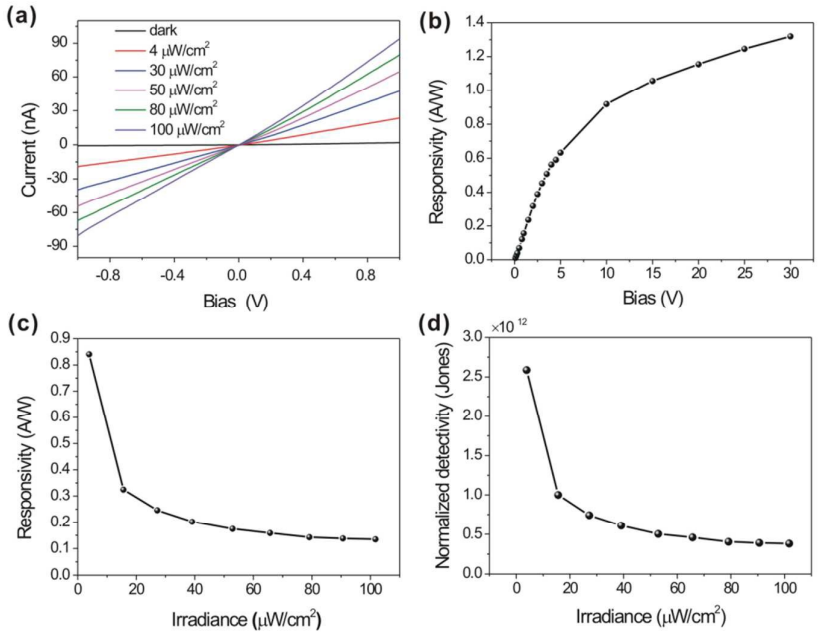

Fig. 7

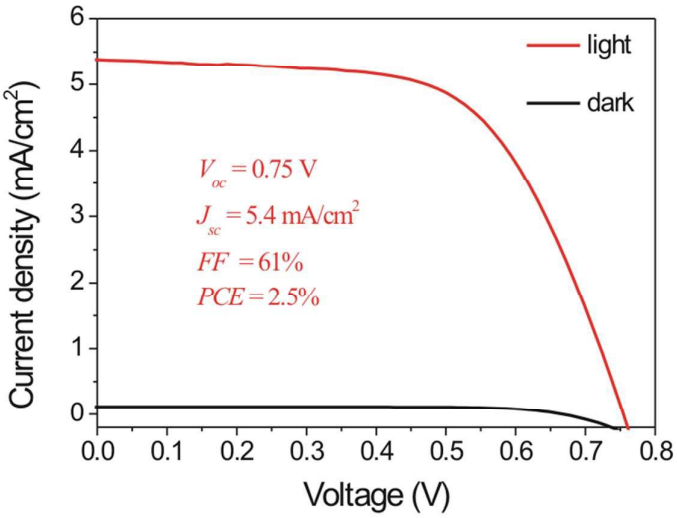

Fig. 8